Application of deconvolution to images from the EGRET gamma-ray telescope

Symeon Charalabides, Andy Shearer, Ray Butler (National University of Ireland, Galway, Ireland)

ABSTRACT

The EGRET gamma-ray telescope has left a legacy of unidentified astronomical sources. Most likely, many of the galactic plane sources will be rotation-powered pulsars. Firm identification has been difficult, given the instrument's poor spatial resolution. The problem is exacerbated by the energy dependant Point Spread Function (PSF) and low numbers of source counts. The main method of identifying sources to-date has been a maximum likelihood method. We have taken a different approach, namely that of regularised deconvolution with a spatially invariant PSF, which is used in optical astronomy and medical X-ray imaging. This technique revealed that wavelet denoising of residuals produced smooth, relatively artefact-free images with improved spatial location. Our source location using standard centroiding produced an improvement in relative spatial location, ranging from 10:1 to 2:1 proportional to source strength. Wavelet deconvolution simultaneously achieves background smoothing, while improving sharpness of the resolved objects. The photon-sparse nature of these images makes them an ideal test bed for such techniques. Although deconvolution does not ordinarily conserve flux, in this instance the flux determination is unaffected in all but the most crowded regions. Finally, we show that the energy dependent PSF can be used to identify objects with a restricted range of energy spectra.

Keywords: Astrometry, Deconvolution, EGRET, Gamma-ray imaging, iMPaIR, Pulsars, Wavelets

1. INTRODUCTION

The EGRET (Energetic Gamma Ray Experiment Telescope) functioned aboard the CGRO (Compton Gamma Ray Observatory) from 22 April 1991 until 9 May 2000, for a total of 9 viewing periods. It detected gamma rays at energies between 20 MeV and 30 GeV by inducing the production of electron-positron pairs, which were subsequently processed to provide the direction of arrival as well as the energy of each photon. The absolute arrival time of photons was recorded to an accuracy of approximately 50 μs. The EGRET had a wide field of view, which spanned almost 80° in diameter, though it operated in a narrow field-of-view mode during viewing periods 5 to 8 in order to conserve the spark chamber gas. However, the sensitivity of the instrument beyond 30° off-axis was down to 15% of that on-axis, and the PSF (Point-Spread Function) degraded equally significantly at this angle. The PSF itself is energy-dependant, with a FWHM (Full-Width, Half-Maximum) of approximately 6° at 100 MeV, which gradually drops for higher energy bands. Although the data gathered by the EGRET have led to important discoveries, there are three major problems associated with the EGRET images. First, although the typical viewing period lasted about two weeks, the number of photons gathered is still low, compared to observations in lower bands of the electromagnetic spectrum. This is partly due to the instrument's architecture: it only captures approximately 35% of photons above 200 MeV. Second, the PSF is not only energy-dependant, but also varies with the angle relative to the instrument's axis: it starts degrading at around 20° and, though the effect is almost always negligible up to 25°, is only reliable up to 30° off-axis. Third, the EGRET images have poor spatial resolution, with each pixel representing an area of 0.5° x 0.5°. Figure 1 shows a fish-net plot of the PSF for the 8 main different energy bands. Figure 2 shows an optical image convolved with the 500 MeV- 1 GeV band PSF. This illustrates the very poor angular resolution of the instrument.

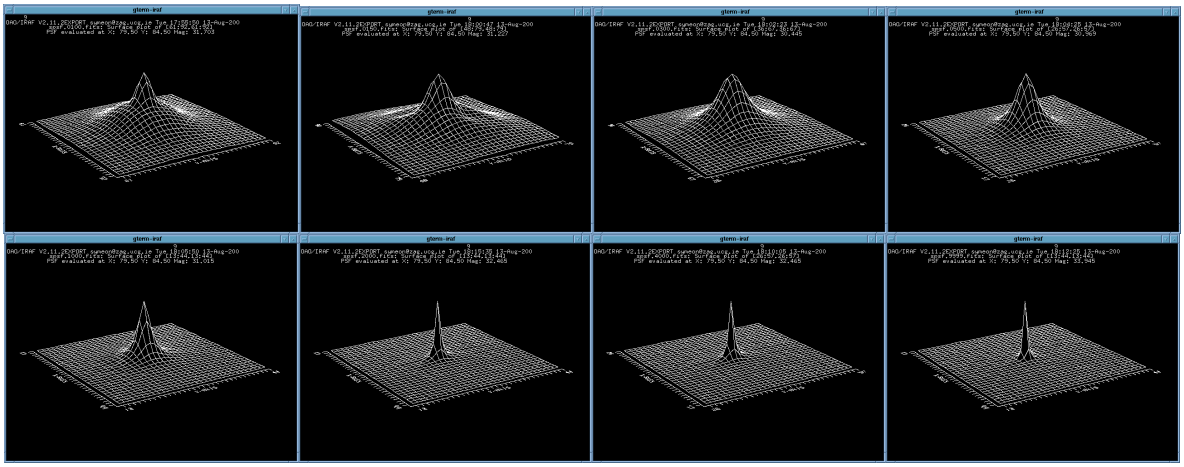

Fig. 1: Observed PSF of EGRET images for the energy bands (top row) 70-100, 100-150, 150-300, 300-500 and (bottom row) 500-1000, 1000-2000, 2000-4000, 4000-10000 MeV, plotted using IRAF, with a grid size of 16°x16°.

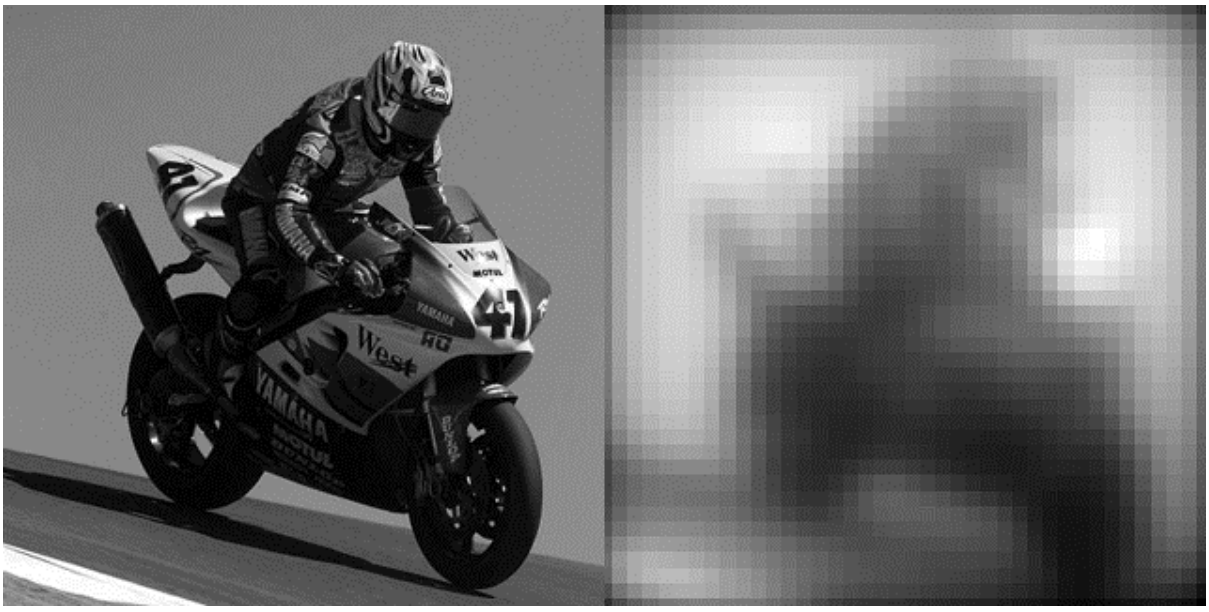

Fig. 2: An optical image, 15° across – effectively the motorcycle is at 2 meters, and how the EGRET would "see" it (Copyright 2000, Gold & Goose)

One of the major EGRET results has been the large number of unresolved sources: the 3rd EGRET catalog (Hartman et al, 1999) lists 66 high-confidence identifications of blazars, 27 lower-confidence potential blazars and 170 unidentified sources out of a total of 271 gamma-ray sources in the energy bands between 100 MeV and 10 GeV. This is due primarily to the poor spatial resolution and the concentration of objects with the galactic plane. Figure 3a shows a composite EGRET image in the 500-1000 MeV range of the region around the Crab pulsar. Figure 3b shows part of this region in the optical – the whole image is smaller than the EGRET PSF for this region. Figures 3c and 3d further enhance in the optical region to demonstrate the massive resolution difference between optical and gamma-ray observations. It is obvious that only bright, well-defined sources will be clearly identified with EGRET images. One

technique has been to look for pulsars – isolated neutron stars with rapid (< 1 second) rotation periods. If we can find in a region of the sky an EGRET signal which is modulated at the same period as a known pulsar in that region, then clearly the source is a pulsar. Seven such objects were identified in this way. Other objects identified include large supernova remnants and active galactic nuclei – the blazars referred to earlier

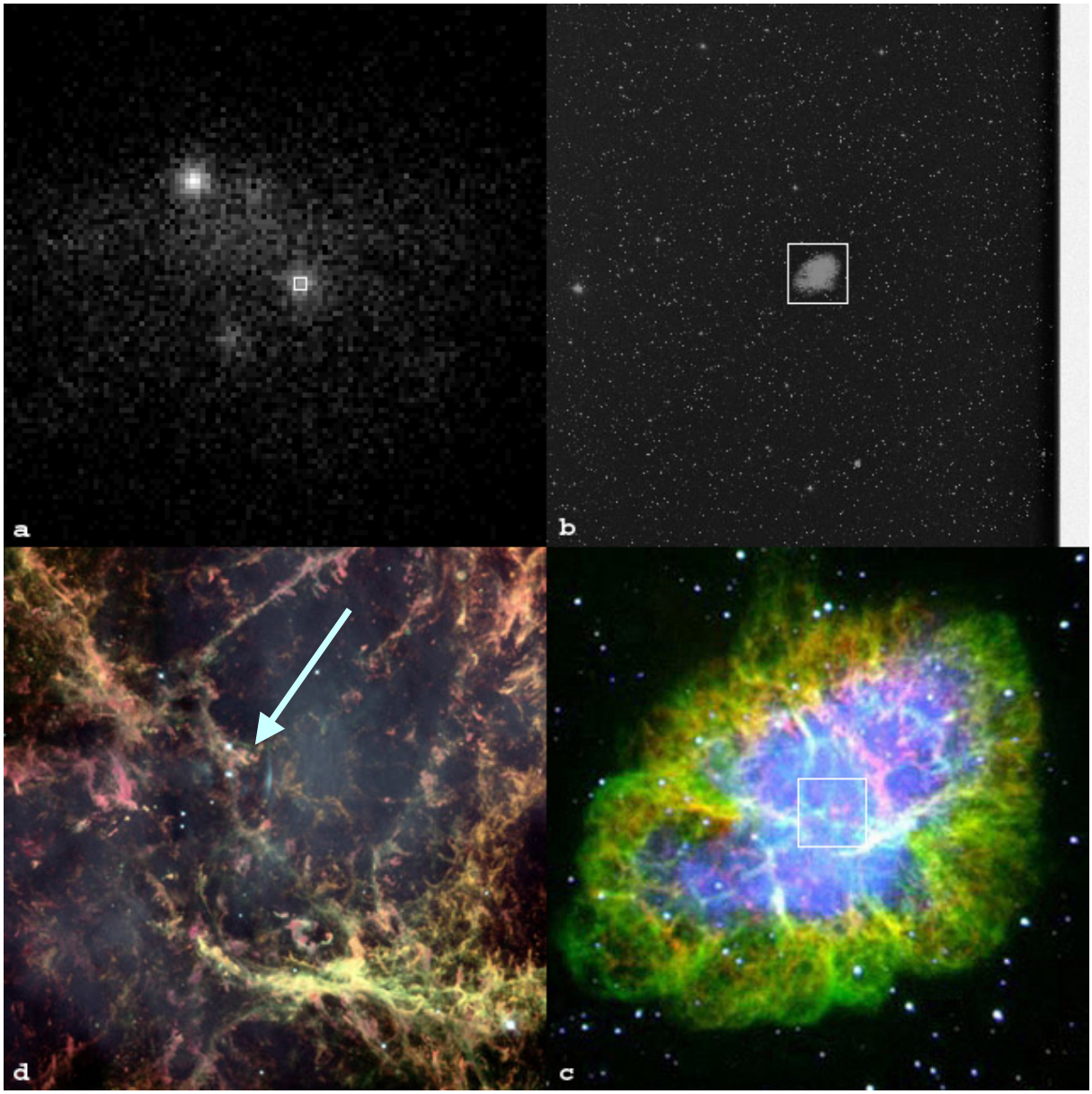

Fig. 3: (a) EGRET image centered at the Crab pulsar. The 1° x 1° square is the same area covered by the optical image (b)
(b) Ground-based optical image from the Digital Sky Survey. The squared area is enlarged on image (c)
(c) Palomar observatory ground-based optical image. Image (d) is a rough enlargement of the squared area.
(d) HST (Hubble Space Telescope) optical image of the inside of the Crab nebula. An arrow points to the Crab pulsar itself, source of the EGRET signal.

2. DECONVOLUTION

2.1 Image Restoration

The process of recovering or estimating the object image *O(x,y)* from an observed image *I(x,y)* in Equation 2.1 is a well studied problem in image processing. When the PSF *P(x,y)* is unknown the problem is referred to as blind deconvolution. In our case however we assume that the PSF is known.

(2.1) $$I(x,y) = O(x,y) * P(x,y) + N(x,y)$$

The process of recovering *O(x,y)* then becomes an inverse problem. Although it is possible to find the inverse of Equation 2.1 by Fourier transform, the result is not satisfactory due to amplification of high frequency noise *N(x,y)*. This type of inverse problem related to image restoration has been the subject of much research in astronomy. The approach adopted by Lucy (1974) derives from the Bayes theorem. The solution given by Equation 2.2 effectively finds an estimate $\psi(x,y)$ that maximizes the likelihood of the observed image *I(x,y)* at each iteration. The *n*th estimate $\psi_n(x,y)$ is given by

(2.2) $$\psi_n(x,y) = \psi_{n-1}(x,y)\left[\frac{I(x,y)}{\psi_{n-1}(x,y) * P(x,y)}\right] * P(-x,-y)$$

The success of this in astronomical image restoration is due in part to the ability to accurately measure the PSF. Likewise the success of this technique in restoration of EGRET images will be determined by the accuracy to which the PSF is measured from a particular source and its applicability to other sources. We should note that this generalized form allows for a spatially variant PSF.

2.2 Regularized Deconvolution

In practice the image restoration algorithm described above suffers from amplification of noise as the number of iterations is increased. At a high enough number of iterations the image begins to break down. In effect noise present in the original image is mistaken for high frequency features. In order to overcome this limitation, Starck and Murtagh (1994) have proposed a regularization technique based on a wavelet denoising algorithm applied to the residual between iterations. The residual, R, is defined as

(2.3) $$R^n(x,y) = I(x,y) - P(x,y) * E^n(x,y)$$

where $E^n(x,y)$ is the object estimate at the *n*th iteration. Specifically, the algorithm performs a hard threshold of the wavelet coefficients of the residual. The threshold level is set by a study of variation of Gaussian noise in this wavelet space. Although the algorithm proposed by Stark and Murtagh is effective, it is computationally demanding due to the redundant *à trous* wavelet transform applied. In addition the method used to set the denoising threshold is based on the assumption of Gaussian noise. In order to improve upon this we have developed an algorithm based on a non-redundant transform - the Daubechies wavelet, (Daubechies 1992), which is more efficient in terms of storage. We denoise the residual between iterations by using a soft thresholding (wavelet shrinkage), which is statistically more attractive then hard thresholding (Donoho1993). We select the level dependent soft threshold as a multiple k of the wavelet coefficient standard deviation. We have developed a parallel spatially variant version of this algorithm, iMPaIR, which is released under a GNU Public Licence.

3. APPLICATION TO EGRET IMAGES

In order to apply the Richardson-Lucy deconvolution with wavelet denoising to the EGRET images, we started by capturing the PSF for the 8 highest out of 10 energy bands. The object we chose as our point of reference was the Vela pulsar (SNR 263.4-03.0) because it has a strong emission in all the gamma-ray energy bands, and there are no other strong point sources inside the 20° circle around it, which might distort the computed PSF. Also, Vela was inside the 25° circle around the instrument's axis a total of 14 times, spanning from the 1st to the 9th viewing period, amounting to a total exposure time of roughly 128 days. This yields good photon statistics which improves the PSF model accuracy. After extracting the PSF, we chose to sub-sample the images to be deconvolved by 3. The images themselves were sub-sampled using a 'nearest neighbour' algorithm, which simply expands each pixel to 9 of the same value. Obviously, we would have to magnify the PSF by the same factor. However, we did this using a linear algorithm which smoothens the PSF curve – given the increased information in the PSF source.

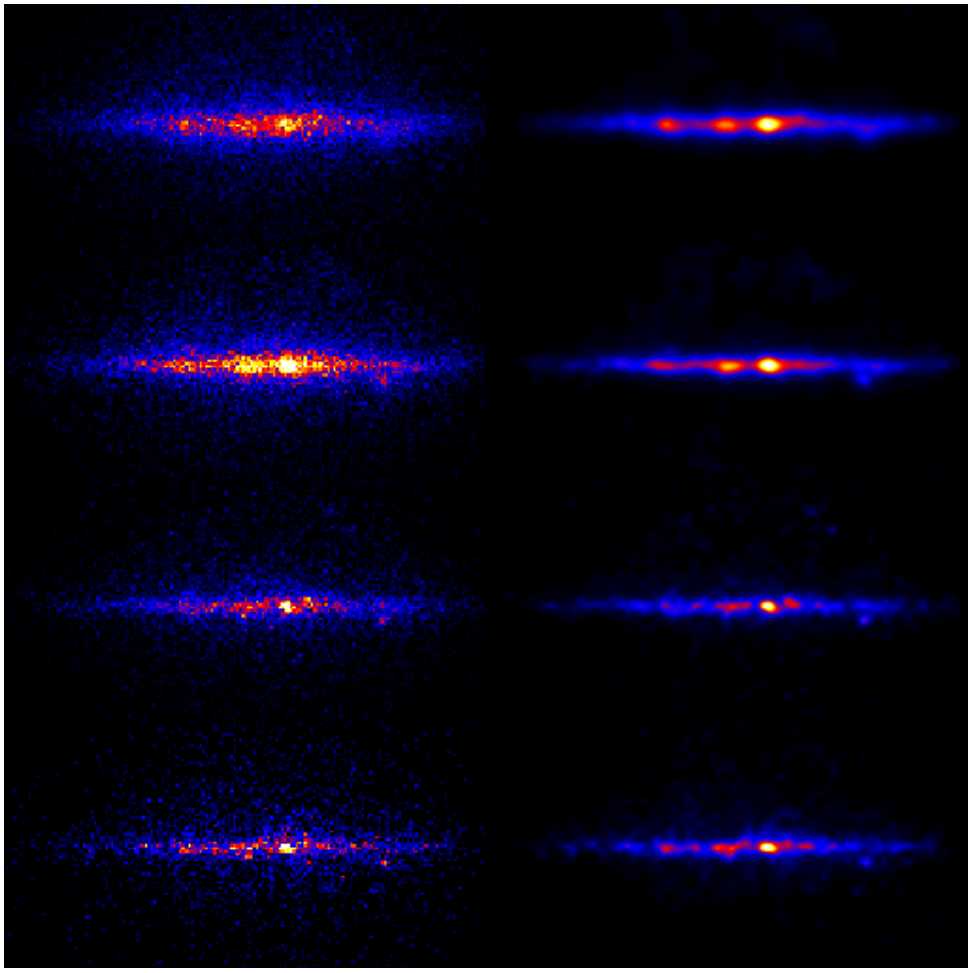

Fig. 4: Galactic centre, before (left) and after (right) deconvolution. The energy bands from top to bottom are: 300-500, 500-1000, 1000-2000, 2000-4000 MeV.

Initially we worked on two distinct images, one centered at Geminga (PSR J0633+1745) and including the Crab pulsar, and one centered at 3EG J1800-2338, which includes the galactic centre. Both images were made by adding all the images with the desired object (centre) within 20° off-axis. The four energy bands with the best signal-to-noise ratio are the 300-500, 500-1000, 1000-2000 and 2000-4000 MeV bands. We deconvolved the chosen images with a number of 15, 10, 5 and 3 iterations respectively, a wavelet level of 3 and a sigma threshold of k=15 for the denoising process. In all cases we used a spatially invariant PSF.

Figures 4 and 5 show the raw and deconvolved images for the region around the galactic centre and Geminga respectively. In both cases the images are subsampled by 3x3 from the original coordinates and cover a region that spans at least 40°x40°. The images have been resized for this illustration and do not demonstrate the full or real improvement achieved. Deconvolution was handled by the iMPaIR software with wavelet denoising. Table 1 shows the error in position for the raw and deconvolved images.

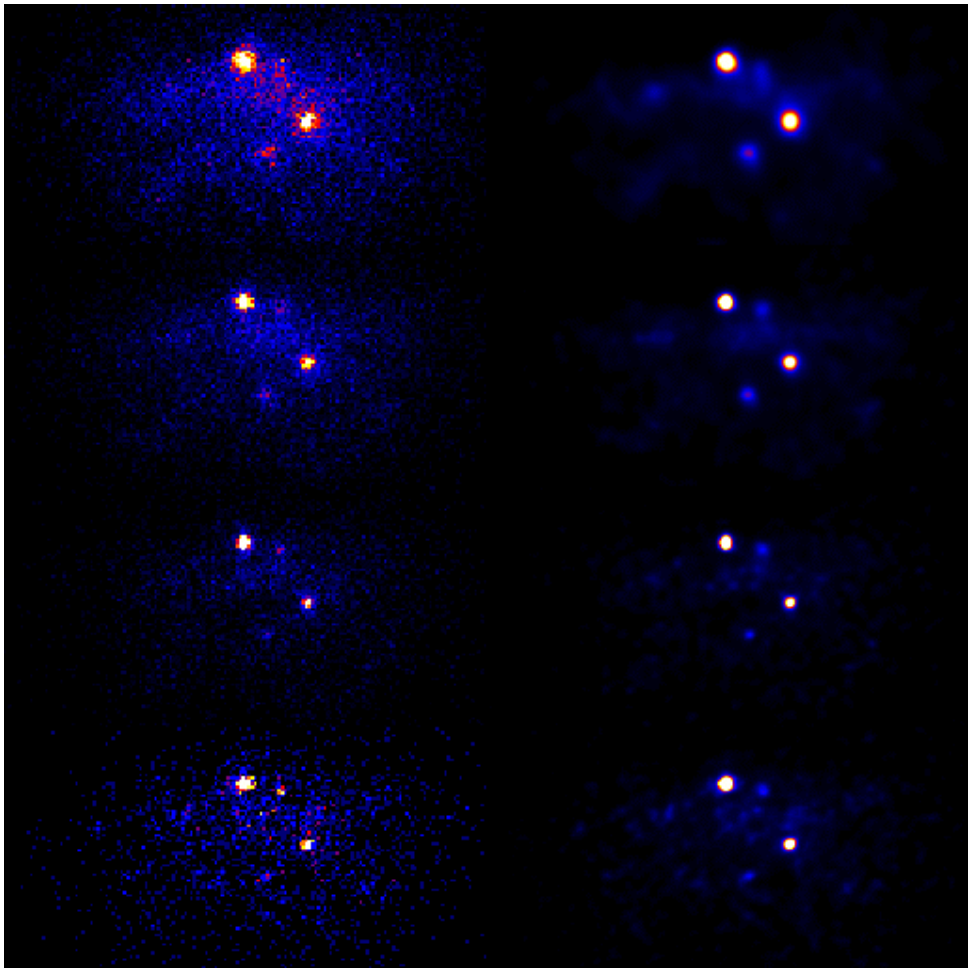

Fig. 5: Geminga and the Crab, before (left) and after (right) deconvolution. The energy bands from top to bottom are: 300-500, 500-1000, 1000-2000, 2000-4000 MeV

Object	Energy	X error (raw)	Y error (raw)	X error (deconvolved)	Y error (deconvolved)
3EG J0534+2200 (Crab)	300-500	0.0398	0.0361	0.0061	0.0105
	500-1000	0.0308	0.0290	0.0066	0.0065
	1000-2000	0.0373	0.0302	0.0057	0.0041
	2000-4000	0.0397	0.0375	0.0062	0.0057
3EG J0617+2238	300-500	0.0319	0.0352	0.0190	0.0453
	500-1000	No source		0.0072	0.0249
	1000-2000	0.0548	0.0521	0.0069	0.0339
	2000-4000	0.0526	0.0554	0.0246	0.0069
3EG J0530+1323	300-500	0.0591	0.0730	0.0068	0.0155
	500-1000	0.0970	0.0695	0.0072	0.0118
	1000-2000	0.0283	0.0391	0.0143	0.0036
	2000-4000	0.0403	0.0481	0.0309	0.0176
3EG J0633+1751 (Geminga)	300-500	0.0459	0.0476	0.0086	0.0109
	500-1000	0.0335	0.0278	0.0051	0.0038
	1000-2000	0.0367	0.0294	0.0043	0.0081
	2000-4000	0.0329	0.0333	0.0044	0.0094
3EG J1746-2851	300-500	0.0625	0.0417	0.0053	0.0008
	500-1000	0.1211	0.0679	0.0034	0.0011
	1000-2000	0.0566	0.0575	0.0099	0.0126
	2000-4000	0.0521	0.0496	0.0147	0.0087
3EG J1733-1313	300-500	0.0452	0.1539	0.0147	0.0017
	500-1000	0.0304	0.0600	0.0106	0.0063
	1000-2000	0.0748	0.0945	0.0182	0.0109
	2000-4000	0.0691	0.0245	0.0159	0.0314

Table 1: Raw and deconvolved positions obtained by fitting a Gaussian profile to the images. The errors are in degrees. Although the PSF of the high energy region is much narrower than that for lower energies (see Fig. 1), the accuracy remains roughly constant due to the much poorer photon statistics in the higher energy regime**.**

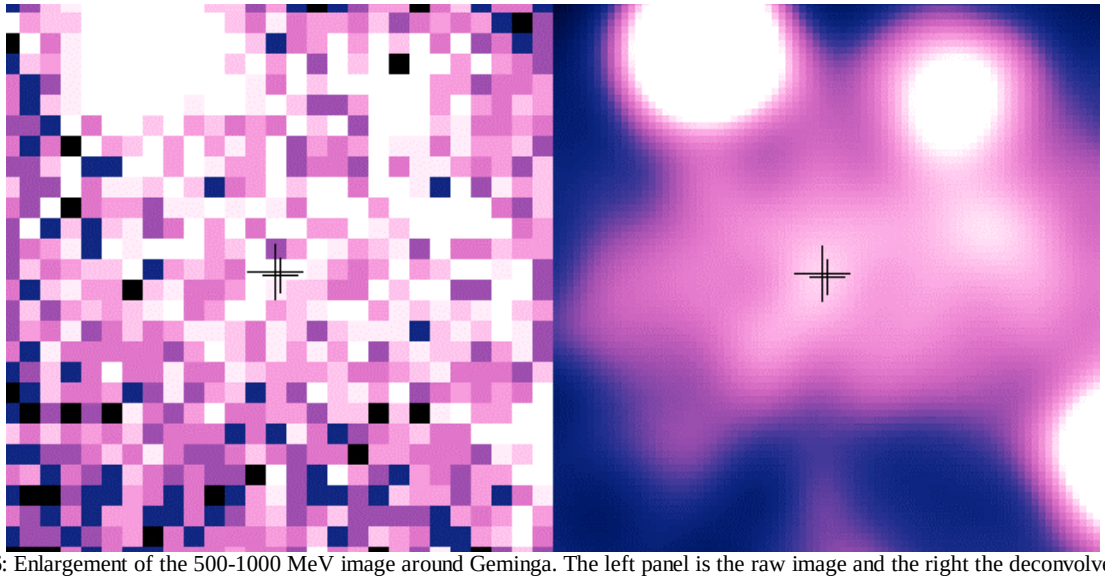

Fig. 6: Enlargement of the 500-1000 MeV image around Geminga. The left panel is the raw image and the right the deconvolved. The large cross marks the projected centre of a Gaussian fit of an area roughly 2° around it and the small cross marks the position of the bright X-ray source 1RXS J060701.4+174202. The distance between them is 0.154 °.

With the improved resolution we are able to look for new EGRET sources. Our approach was to search for sources with at least a 5-sigma signal in all energy bands. For example in the Geminga region we have identified a new candidate EGRET object coincident with the ROSAT object 1RXS J060701.4+174202. Figure 6 shows the raw and deconvolved 500-1000 MeV image with the position of the X-ray source marked as the small cross. Positive identification of a source will require consideration of the physics of the sources (primarily the energy spectrum) as well as positional coincidence.

4. CONCLUSION AND FUTURE WORK

We have shown that regularised deconvolution makes a 5-fold improvement in positional accuracy for the brighter EGRET sources. This is despite the poor photon statistics and for all major energy bands. Our final average 1-sigma error margin is about 30". The next stage in this work will be to apply a spatially variant PSF to the images using the iMPaIR software. Application of this to all photons from the EGRET database will enable us to determine a better astrometric framework to search for the candidates to fainter sources. We will also have to investigate the effect of deconvolution of sparse images with poor photon statistics and with a rapidly varying and energy dependent PSF. The result will be the Galway EGRET Catalog which should be finished in early 2003 in time for the first results from the Integral Gamma Ray satellite due to be launched in October 2002.

ACKNOWLEDGEMENTS

The authors wish to acknowledge the financial support of Enterprise Ireland. We are also grateful to Seth Digel and Chris Shrader of the Compton CGRO Space Observatory for being able gatekeepers of the EGRET archives and a nice poster. Lastly, our sincerest admiration goes to the Greek military drafting policy.

REFERENCES

Daubechies I., "Ten lectures on Wavelets", Society for Industrial and Applied Mathematics, 1992

Donoho D. L., "Nonlinear wavelet methods for recovery of signals, densities, and spectra from indirect and noisy data", IEEE Transaction on Information Theory 39, pp. 257-260, 1993

Hartman et al, "The Third EGRET Catalog of High-Energy Gamma-Ray Sources", Astrophysical Journal Supplement Series 123, Issue 1, pp. 79-202, 1999

Lucy L. B., "An iterative technique for the rectification of observed distributions", Astrophysical Journal 79, pp. 745, 1974

Magain P., Courbin F., Sohy S., "Deconvolution with correct sampling", The Messenger, 88, 28-31, 1997

Richardson W. H., "Bayesian-based iterative method of image restoration", Optical Society of America Journal 62, pp. 55-59, 1972

Starck J-L., Murtagh, F., "Image restoration with noise suppression using the wavelet transform", Astronomy and Astrophysics 288, no. 1, pp. 342-348, 1994